STARS

University of Central Florida
STARS

Electronic Theses and Dissertations, 2004-2019

2007

Scanning Fabry-perot Spectrometer For Terahertz And Gigahertz Spectroscopy Using Dielectric Bragg Mirrors

Justin Cleary
University of Central Florida

Part of the Physics Commons
Find similar works at: https://stars.library.ucf.edu/etd
University of Central Florida Libraries http://library.ucf.edu

This Masters Thesis (Open Access) is brought to you for free and open access by STARS. It has been accepted for inclusion in Electronic Theses and Dissertations, 2004-2019 by an authorized administrator of STARS. For more information, please contact STARS@ucf.edu.

STARS Citation
Cleary, Justin, "Scanning Fabry-perot Spectrometer For Terahertz And Gigahertz Spectroscopy Using Dielectric Bragg Mirrors" (2007). *Electronic Theses and Dissertations, 2004-2019*. 3120.
https://stars.library.ucf.edu/etd/3120

University of Central Florida
STARS
Showcase of Text, Archives, Research & Scholarship

SCANNING FABRY-PEROT SPECTROMETER FOR TERAHERTZ AND GIGAHERTZ SPECTROSCOPY USING DIELECTRIC BRAGG MIRRORS

by

JUSTIN CLEARY
B.S. University of Central Florida, 2005

A thesis submitted in partial fulfillment of the requirements
for the degree of Masters of Science
in the Department of Physics
in the College of Sciences
at the University of Central Florida
Orlando, Florida

Spring Term
2007

Major Professor: Robert E. Peale

© 2007 Justin Cleary

ABSTRACT

A scanning Fabry-Perot transmission filter composed of a pair of dielectric mirrors has been demonstrated at millimeter and sub-millimeter wavelengths. The mirrors are formed by alternating quarter-wave optical thicknesses of silicon and air in the usual Bragg configuration. Detailed theoretical considerations are presented for determining the optimum design including factors that affect achievable finesse. Fundamental loss by lattice and free carrier absorption are considered. High resistivity in the silicon layers was found important for achieving high transmittance and finesse, especially at the longer wavelengths. Also considered are technological factors such as surface roughness, bowing, and misalignment for various proposed manufacturing schemes. Characterization was performed at sub-mm wavelengths using a gas laser together with a Golay cell detector and at millimeter wavelengths using a backward wave oscillator and microwave power meter. A finesse value of 422 for a scanning Fabry-Perot cavity composed of three-period Bragg mirrors was experimentally demonstrated. Finesse values of several thousand are considered to be within reach. This suggests the possibility of a compact terahertz Fabry-Perot spectrometer that can operate in low resonance order to realize high free spectral range while simultaneously achieving a high spectral resolution. Such a device is directly suitable for airborne/satellite and man-portable sensing instrumentation.

ACKNOWLEDGMENTS

This work was supported in part by an NASA SBIR Phase I NNC06CB23C to Zyberwear, by a matching grant from the Florida High Technology Corridor program, by an ASEE summer faculty fellowship for R. E. Peale at AFRL/SNHC Hanscom AFB, and by an AFRL contract FA871806C0076. I would also like to acknowledge the contributions to this work from the following people: Robert E. Peale, Chris J. Fredricksen, Andrei V. Muravjov, Jasen Enz, Maxim V. Dolguikh, Todd W. Du Bosq, William R. Folks, Sidhartha Pandey, Glenn Boreman, Ravi Todi, Kalpathy Sundaram and Oliver Edwards.

TABLE OF CONTENTS

LIST OF FIGURES vi

LIST OF TABLES vii

CHAPTER ONE: INTRODUCTION 1

CHAPTER TWO: THEORETICAL 6

General Fabry-Perot Relations: 6

Matrix Calculation Method: 9

Extinction Coefficient Calculations 10

Theoretical Simulations 14

Finesse Degradation 19

CHAPTER THREE: EXPERIMENTAL DETAILS 22

Chemical Etching 22

Fabry-Perot Setup 23

CHAPTER FOUR: DATA ANALYSIS 25

Fabry-Perot Spectra 25

Chemical Etchcing Results and Finesse Factors 30

CHAPTER FIVE: DISCUSSION 35

APPENDIX: EXPERIMENTAL EQUIPMENT 41

REFERENCES 44

LIST OF FIGURES

Figure 1: Scanning Fabry-Perot system described in this work. 2
Figure 2: Transmission spectrum for Fabry Perot spectrometer with finesse of ~300. 4
Figure 3: The extinction coefficient of silicon due to lattice absorption. 12
Figure 4: Total extinction coefficient. 14
Figure 5. Reflectance spectrum for a Bragg mirror composed of different numbers of periods. 15
Figure 6: Semilog plot of finesse and reflectance vs. number of periods for λ = 136.8 μm.. 15
Figure 7: Semilog plot of finesse and reflectance vs. number of periods for λ = 3.7 mm. 16
Figure 8: Resistivity dependence of Fabry-Perot resonance.. 18
Figure 9: Full-width half-maximum as a function of the extinction coefficient and resisitivity.. 19
Figure 10: Experimental (solid) and theoretical (dotted) Fabry-Perot resonance........................ 26
Figure 11: Experimental (solid) and theoretical (dotted) data at a wavelength of 134.00 μm. ... 28
Figure 12: Experimental (solid) and theoretical (dotted) data at a wavelength of 109.29 μm. 29
Figure 13: Depth profiling image for 60 minute patterned etch on <111> oriented silicon. 32
Figure 14: Image for 60 minute patterned etch on <100> oriented silicon. 32
Figure 15: Theoretical finesse values vs. wavelength. 37
Figure 16: Empirical finesse values vs. wavelength. 38
Figure 17: Measured reflectance of a silicon Bragg mirror compared to other authors. 39
Figure 18: Fabry-Perot on Thorlabs LNR50S TravelMax with Golay cell detector. 42
Figure 19: Far-infrared DEOS gas laser. 42
Figure 20: Siemens Backward Wave Oscillator (tunable millimeter wavelength source). 43
Figure 21: Microwave power meter and attenuator. 43

LIST OF TABLES

Table 1: Specifications for mirror design. 24
Table 2: Estimated finesse factors for 100 μm wavelength. 35
Table 3: Estimated finesse factors for 3 mm wavelength. 35

CHAPTER ONE: INTRODUCTION

The objective of this work was to develop the core technology for a compact scanning Fabry-Perot spectrometer, for satellite far-infrared astronomy[1,2] and Earth remote sensing,[3] that operates at wavelengths of $\lambda = 100$ μm and longer, with a resolving power up to 10,000 and free spectral range of up to $\lambda / 2$. This objective requires development of dielectric Fabry-Perot mirrors having up to 99.996% reflectance at sub-mm wavelengths to enable the unprecedented system finesse. The standard mirror used in scanning Fabry-Perots at sub-mm wavelengths has been metal mesh.[4] Others[5-9] have already reported multilayer dielectric mirrors based on silicon, but without a precise measurement of achieved reflectivity and not applied to the application of a scanning Fabry-Perot. In this work, multilayer mirrors with up to three periods of silicon separated by air were combined into a scanning Fabry-Perot system. The measured finesses are somewhat below those of the best mesh-based systems in this preliminary study, though calculations indicate they can be higher. This discrepancy can be attributed to inaccuracies in the spacing between the delicate multilayer silicon filters and other technological factors. The measured finesse values give an accurate lower bound on the achieved Bragg mirror reflectivity. Figure 1 presents the "scanning" Fabry-Perot setup described in this work. The source could be anything including any astronomical source. If the source is non-monochromatic, a pre-filter is required. The Fabry-Perot etalons are separated by some gap of distance *d*. The transmitted light is then passed to the detector.

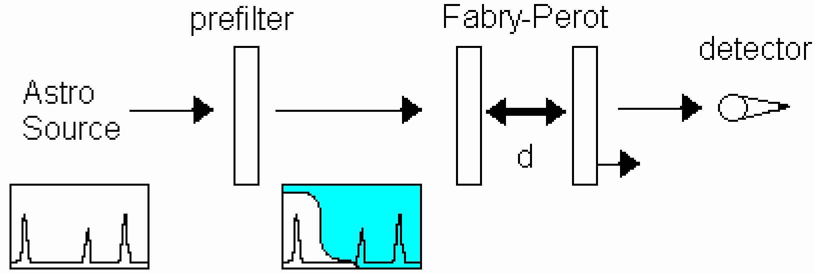

Figure 1: Scanning Fabry-Perot system described in this work.

One mirror is fixed and the second mirror moves in order to observe transmission resonances at a constant wavelength.

A clean solid silver mirror can have a maximum reflectivity of 99.56 % at a wavelength of 100 μm, as determined by the real part of the surface impedance of the metal,[10]

$$R = 1 - \frac{4}{\mu_o c}\sqrt{\frac{\omega \mu_o}{2\sigma}} \quad , \tag{1}$$

where μ_o is the permeability constant, c is the speed of light, σ is the DC conductivity and ω is the angular frequency. Confocal cavity Fabry-Perot spectrometers and filters based on solid metal mirrors have achieved finesse values up to a few thousand at millimeter wavelengths,[11-13] but such designs appear to be impractical at sub-mm wavelengths. Standard art for the past several decades in airborne or satellite Fabry-Perot spectrometers has been flat metal mesh mirrors.[4, 14-24] Empirical reflectivities of such mirrors at sub-mm wavelengths typically does not exceed 97% or 99.8% for mm wavelengths, so that the finesse of Fabry-Perot cavities based on them has been $< \sim 100$ in the sub-mm range[4, 14-24] and $< \sim 2000$ at millimeter wavelengths[12, 25-26].

Mesh mirrors have limited spectral range compared to what might be achieved using dielectric mirrors[5-9], the approach investigated here.

Vacuum deposited dielectric multi-layer Bragg mirrors known in the near-IR and visible range, which give reflectivity exceeding 99.99%, have been unattainable in the far-IR due to strong absorption by glassy layers. Therefore, to obtain resolving powers Q of 10,000 (where the resolution at 100 cm^{-1} would be comparable to that of a high-end Fourier spectrometer, i.e. 0.01 cm^{-1}) astronomers have operated their Fabry-Perot spectrometers at high interference order k.[14-15] Values for k of several hundred are typical. Unfortunately, this reduces the free spectral range (FSR) of the instrument. At 100 μm wavelength and k = 100, the free spectral range is only 1 μm of wavelength. To avoid contamination of the spectrum by signal at wavelengths passed by neighboring resonances, narrow band filters have been required to limit the spectral range to a single resonance. In the Far-IR, the filter has been a grating monochromator,[14] because sharp narrow-band interference filters based on multiple thin films are unavailable at those wavelengths. This adds considerable bulk and complexity to the system.

To illustrate the challenge more clearly, figure 2 presents calculated transmittance spectra for a Fabry-Perot cavity with mirrors having R = 99%. This corresponds to a finesse of ~300 (which is already much better than known far-IR Fabry-Perot spectrometers). Two different mirror spacings are considered, 50 and 500 μm. The former shows a 1st order transmission resonance at 100 cm^{-1}, where the free spectral range is about 50 cm^{-1}. Unfortunately, the transmission line width exceeds 10 cm^{-1}, usually an insufficient resolution for molecular spectroscopy. For the larger cavity, the instrument would operate in 10th order at 100 cm^{-1}. The transmission linewidth has improved to ~1 cm^{-1} (though still inadequate for many purposes), but

the free spectral range has been reduced to ~10 cm^{-1}, and a complex filter solution would be required. A goal of this investigation is to operate in as low of a resonance order possible to avoid this problem.

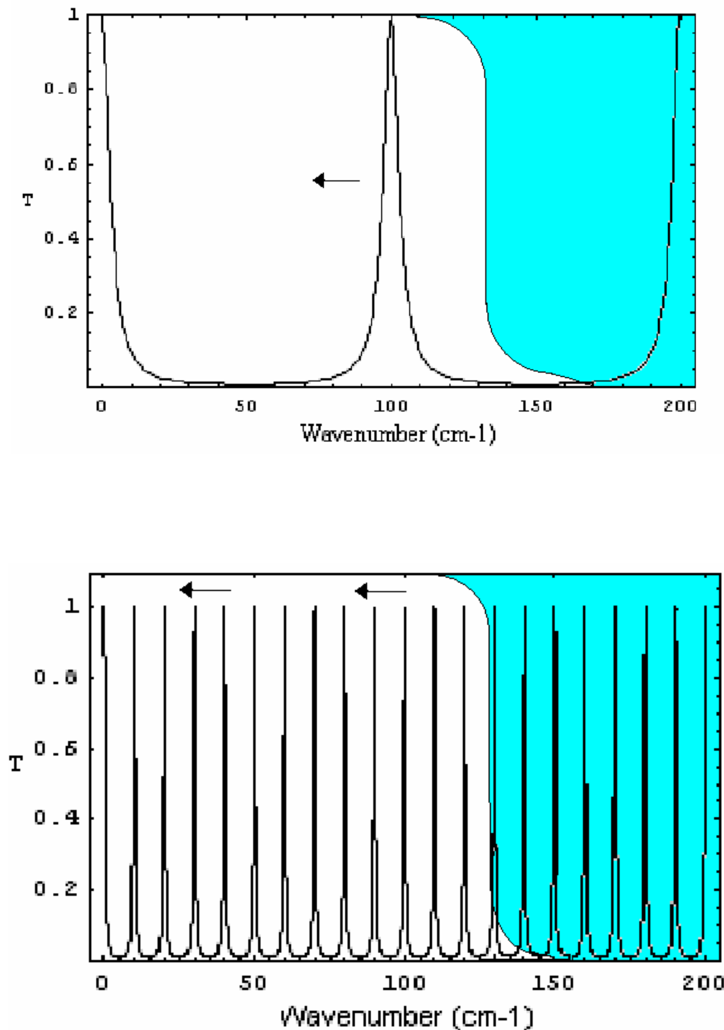

Figure 2: Transmission spectrum for Fabry Perot spectrometer with finesse of ~300.

Calculations correspond to mirror reflectivity of 99%. (Top) Cavity length = 50 µm. (Bottom) Cavity length = 500 µm. The arrows indicate the movement of transmittance resonances with Fabry-Perot cavity widening. The blue shading indicates regions blocked by a possible pre-filter.

To design high-reflectivity mirrors for a high finesse scanning Fabry-Perot spectrometer, we consider Bragg mirrors, which consist of alternating layers with large index contrast and optical thicknesses equal to one quarter of the intended center-wavelength. In the usual Bragg mirror configuration, the silicon layers would have an optical thickness of one quarter of the wavelength, giving a physical thickness of ~ 7 μm at 100 μm free space wavelength. Each such silicon layer (period) in the Bragg stack would be separated by a 25 μm gap. This work considers the limitations posed by the achievable manufacturing tolerances. Fundamental optical losses due to free carrier and lattice absorption are also considered.

Various procedures have been considered to create quarter-wave Bragg stacks out of silicon wafers. The simplest is to separate silicon layers by mechanically independent spacers.[5-7, 9] Silicon Bragg stacks have also been created by laser drilling and deep reactive ion etching.[8] Chemical etching and a photoresist process are considered here.

The theoretical maximum finesse is usually determined from the reflectivity of each of the cavity mirrors. Experimental finesse values are determined from the widths of the observed transmittance resonances, and they are nearly always significantly less than predicted for reasons that have been thoroughly explored.[27] Besides fundamental loss mechanisms, such as absorption and scattering, technological factors such as mirror-surface roughness, lack of mirror flatness (bowing), and mirror misalignment are strongly limiting technological factors.

CHAPTER TWO: THEORETICAL

General Fabry-Perot Relations:

Fabry-Perot spectrometers are characterized by their transmittance resonances. Most papers written on theoretical Fabry-Perot systems contain calculations using the Airy function for transmittance. This transmittance is[28]

$$T = [1 + \frac{A}{T_o}]^{-2} \quad [1 + \frac{4R_o}{(1 - R_o)^2} \sin^2(\frac{\delta}{2})]^{-1} . \tag{2}$$

Here R_o, T_o and A are the reflectance, transmittance and absorbance values for one mirror, respectively and δ is a phase shift upon passing through the interfaces, which will described below. This equation is derived from the relation between the incident electric field and the multiple electric field waves transmitted through an interface. A full derivation of the Airy function can be seen in *Optics* by Hecht.[28] The absorbance, assumed small, is[18]

$$A \approx 1 - T_o - R_o . \tag{3}$$

Using geometry, it can be shown that the path length difference of successive waves transmitted through the mirror undergo a path length difference of

$$\Lambda = 2 n_m d \cos(\theta_t) \ , \tag{4}$$

where n_m is the refractive index of the material between the mirrors, d is the spacing between mirrors and the θ_t is the incident angle from the normal. Transmittance maxima occur when the path length difference is

$$\Lambda = k\lambda , \tag{5}$$

where k is the integer resonance order of the transmission peak. The phase difference of successive transmitted waves is 2π multiplied by the integer resonance order, which is then rewritten using equations 4 and 5 as

$$\delta = 2\pi k = \frac{4n_m d\cos(\theta_t)}{\lambda}\pi \quad . \tag{6}$$

Upon the assumption of normal incidence and the material between the mirrors being air, a relation comparing the resonance order, wavelength and mirror separation is found;

$$k\lambda = 2d \; . \tag{7}$$

For the special case of first order ($k = 1$), where $d = L$ which is the length of separation between the mirrors at the first resonance. Further resonances can be seen at multiples of the distance L from the first order resonances. Equation 7 then shows that transmission peaks of a scanning Fabry-Perot spectrometer are separated by

$$L = \frac{\lambda}{2} \; . \tag{8}$$

Equation 7 also results in another important relation concerning the corresponding full-width half-maximums $\Delta\lambda$ and Δd;

$$k\Delta\lambda = 2\Delta d \quad . \tag{9}$$

Finesse is the “number of resolvable spectral lines”[29] and is often used to describe the sharpness of the transmission peaks in Fabry-Perot spectrometers. Finesse is defined as the ratio of the full phase between peaks per the full-width half-maximum of the phase.

$$F_R \equiv \frac{2\pi}{FWHM} \, . \tag{10}$$

From Equation 2, the change in phase from the center of the peak to the half-transmittance point is found to be

$$\Delta\delta_{\frac{1}{2}} = 2\arcsin\left(\frac{1-R_o}{2\sqrt{R_o}}\right) \tag{11}$$

The full-width half-maximum is then two multiplied by this phase difference. This value is used to calculate finesse and an approximation is made for the reflectance of the Fabry-Perot mirror being greater than ~60%.

$$F_R = \frac{\pi}{2\arcsin\left(\frac{1-R_o}{2\sqrt{R_o}}\right)} \approx \frac{\pi\sqrt{R_o}}{1-R_o}. \tag{12}$$

The resolving power Q is defined.

$$Q \equiv \frac{d}{\Delta d} = kF \quad . \tag{13}$$

An equation for finesse in terms of the wavelength and full-width half-maximum of a scanning Fabry-Perot Δd is found using equations 7-9 and 13 to be

$$F = \frac{L}{\Delta d} = \frac{\lambda}{2\Delta d}. \tag{14}$$

The free spectral range of the Fabry-Perot spectrometer (as discussed in the introduction) is

$$FSR = \frac{\lambda}{k}. \tag{15}$$

Matrix Calculation Method:

The reflectivity of the Bragg mirrors used in this study is determined from the standard matrix formulation of the boundary conditions at the film interfaces found from Maxwell's equations.[29-30] The amplitude of the reflection coefficient r is

$$r = \frac{E_m - H_m}{E_m + H_m} \quad , \tag{16}$$

and the amplitude of the transmission coefficient t is

$$t = \frac{2}{E_m + H_m} \quad , \tag{17}$$

where

$$\begin{pmatrix} E_m \\ H_m \end{pmatrix} = M \begin{pmatrix} 1 \\ 1 \end{pmatrix} . \tag{18}$$

E_m and H_m are tangential components of the electric field and magnetic field, and M is the product matrix of L layers. In our specific case both the incident medium and the medium behind the mirror are air. M is given by

$$M = M_L M_{L-1} \cdots M_j \cdots M_2 M_1 \quad , \tag{19}$$

where M_j represents the jth layer of the Bragg mirror and has the form

$$M_j = \begin{pmatrix} \cos\delta_j & \frac{i}{\eta_j}\sin\delta_j \\ i\eta_j \sin\delta_j & \cos\delta_j \end{pmatrix} . \tag{20}$$

In equation 20 the phase for normal incidence (half of the phase in equation 6) is

$$\delta_j = \frac{2\pi}{\lambda}\left(\eta_j d_j\right), \tag{21}$$

and the complex refractive index is

$$\eta_j = \eta'_j - i\eta''_j \quad , \tag{22}$$

where η'_j is the real index of refraction and η''_j the extinction coefficient of the jth layer. Values for η'_j of silicon are tabulated for wavelengths out to 333 μm,[31] and we linearly extrapolate these data for wavelengths out to 7 mm. Our method of estimating η''_j is discussed in the next sub-section. The reflectivity for one mirror to be used in equation 12 is

$$R = |r|^2 \ . \tag{23}$$

The transmittance for Fabry-Perot spectrometers using multilayer films is

$$T = |t|^2 \ . \tag{24}$$

Extinction Coefficient Calculations

Predicting the effects of losses on Fabry-Perot cavity finesse requires accurate knowledge of η''. The effects of different loss mechanisms are additive in η''. The contribution from lattice absorption is estimated using a fit to empirical wavelength-dependent absorption coefficients α for room-temperature silicon. The extinction coefficient is then found according to

$$\eta'' = \frac{c\alpha}{2\omega}, \tag{25}$$

where α is the absorption coefficient. Unfortunately, the available data for α in the literature is rather uncertain. Figure 3 plots the absorption coefficient for silicon from data of Loewenstein et al[31] and Bruesch.[32] One sees that the discrepancy between these data sets exceeds a factor 7 beyond 100 μm wavelength, which coincides with the spectral region of interest. One also sees that the η'' values determined from the Loewenstein data rise with wavelength λ, but this is unphysical behavior for lattice absorption: Absorption by phonons should fall with the phonon density of states as λ^{-2}, so that η'' should fall like λ^{-1} according to equation 25. The Loewenstein data are surely contaminated by free carrier absorption, the absorption coefficient of which rises as λ^2 so that η'' rises as λ^3. Thus we take the Bruesch data to be the most accurate representation of losses due to lattice absorption.

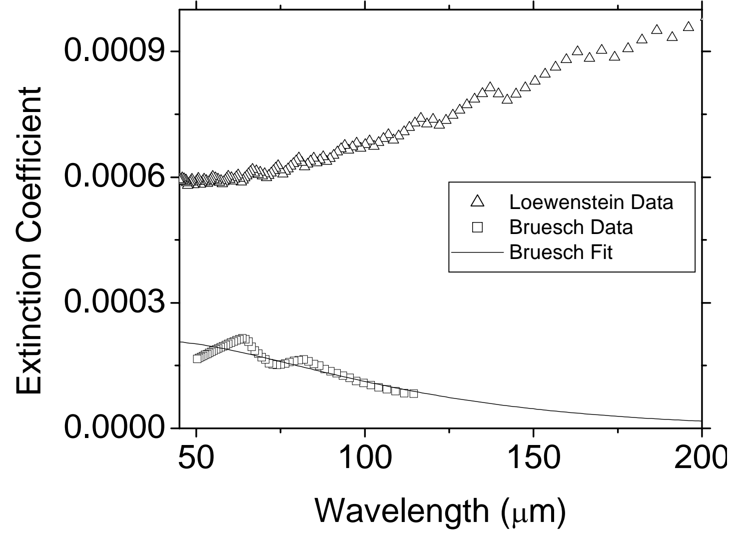

Figure 3: The extinction coefficient of silicon due to lattice absorption.

The upper data set is calculated from the absorption coefficient published by Loewenstein et al.,[31] while the lower data set is from Bruesch.[32] Only the lower data set has physically reasonable wavelength dependence for lattice absorption.

The free carrier contribution the extinction coefficient is found by calculating the free carrier absorption coefficient for room temperature silicon. The free carrier absorption is calculated for semiconductors by[33-34]

$$\alpha_f = \frac{Nq^2\tau}{\varepsilon_o c\eta' m^*\left(1+\omega^2\tau^2\right)} \quad , \tag{26}$$

where N is impurity concentration, q is the electron charge, m^* is the effective mass of the charge carriers and τ is the mean relaxation time of the charge carriers. The effective mass for positive or negative charge carriers in silicon was calculated based on the longitudinal and transverse effective mass.[35] Equation 26 gives the well known λ^2 dependence in the sub-mm wavelength region, where $\omega\tau$>>1. At millimeter wavelengths this relation approaches a constant.

With the resistivity and dopant type known for the silicon, the carrier concentration and mobility (μ) were found using empirical values.[35] The mobility was then used to calculate the relaxation time according to

$$\mu = \frac{q\tau}{m^*}. \tag{27}$$

The value calculated for relaxation time from empirical mobility values was then used to calculate the free carrier part of the absorption coefficient with equation 26. This absorption coefficient was then used with equation 25, in conjunction with the lattice absorption coefficient in order to estimate the total extinction coefficient.

For n-type silicon, the extinction coefficient is plotted in figure 4 for different resistivity values. In the sub-mm regime, the free carrier contribution can be small compared to the lattice contribution for resistivity ≥ 1,000 Ω-cm. In the millimeter wavelength range, free carrier absorption always dominates, implying that the highest available resistivity is essential to achieving high finesse.

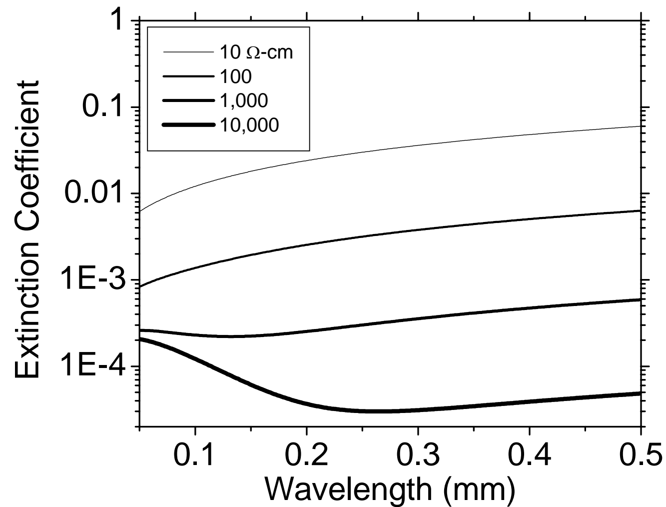

Figure 4: Total extinction coefficient.

Includes both lattice (Bruesch values) and free carrier absorption for n-type doped silicon at various resistivities. At wavelengths near 100 μm, the contribution of free carriers to the total loss is relatively small compared with that of lattice absorption when the resistivity is higher than ~1000 Ω-cm.

Theoretical Simulations

Reflectivity spectra are calculated for Fabry-Perot mirrors designed for a wavelength of 136.8 μm. The simulated silicon is n-type with 10,000 Ω-cm resistivity. The simulations include Bragg stacks of 10 μm thick silicon and 34.2 μm airgaps. As seen in figures 5 and 6, a reflectivity using six period mirrors of 99.996% is reached corresponding to a finesse value of roughly 78,000. Further simulations show that six periods will achieve approximately the highest possible finesse value for this system and going beyond this will not have any real advantage.

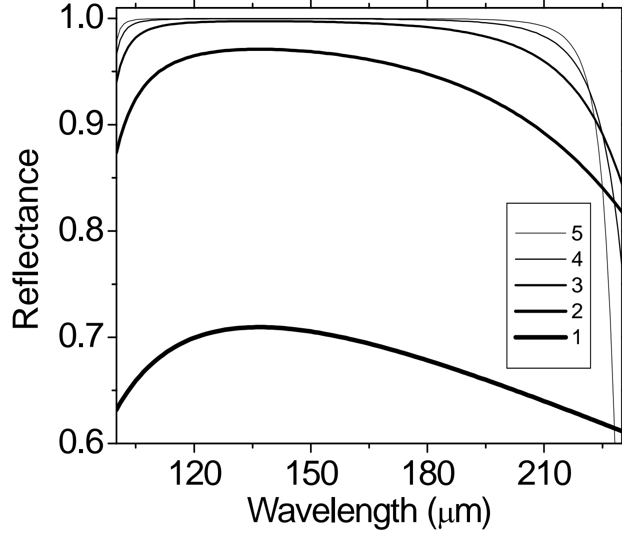

Figure 5. Reflectance spectrum for a Bragg mirror composed of different numbers of periods.

Each period contains a 10 μm silicon wafers.

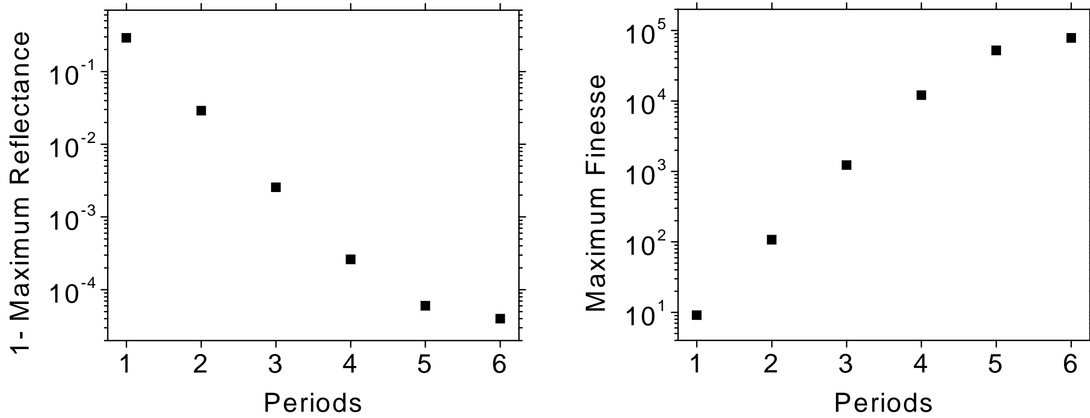

Figure 6: Semilog plot of finesse and reflectance vs. number of periods for $\lambda = 136.8$ μm..

(Left)1-maximum reflectance versus periods. (Right) Maximum finesse versus periods.

A similar investigation for n-type silicon with 10,000 Ω-cm resistivity at millimeter wavelengths yields similar results. Calculations were completed for a wavelength of 3.7 mm using silicon Bragg mirrors with 270 μm thick silicon and 923.4 μm thick airgaps. As seen in figure 7, the maximum reflectivity for this ideal calculation with six periods is 99.981%, which corresponds to a maximum finesse of approximately 16,500. As with the case for the sub-millimeter simulation, the finesse saturates at six periods but at a much lower finesse value due to the extra absorption from the thicker silicon.

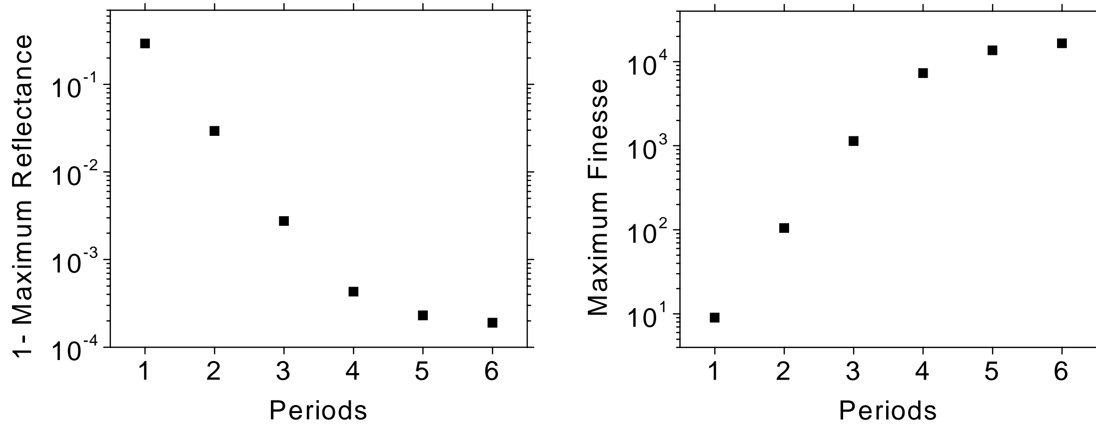

Figure 7: Semilog plot of finesse and reflectance vs. number of periods for λ = 3.7 mm. (Left)1-maximum reflectance versus periods. (Right) Maximum finesse versus periods.

Once the reflectivity spectrum is known, we next calculate the transmittance of the scanning Fabry-Perot at fixed optical frequency as a function of the variable gap between the cavity mirrors. These resonance spectra may be compared with the experimental data we obtain

using various monochromatic millimeter and sub-mm wave sources. See the optical characterization results in chapter four.

Figure 8 reveals the effect of free carrier absorption on a Fabry-Perot transmission resonance. The calculated first order resonance of a Fabry-Perot cavity having single-period Bragg mirrors formed of silicon with different resistivities for both millimeter and sub-mm design wavelengths is presented. It is clear that only resistivity of at least 1000 Ω-cm is acceptable at millimeter wavelengths, while rather high resistivity (100 Ω-cm) is still desirable at sub-mm wavelengths.

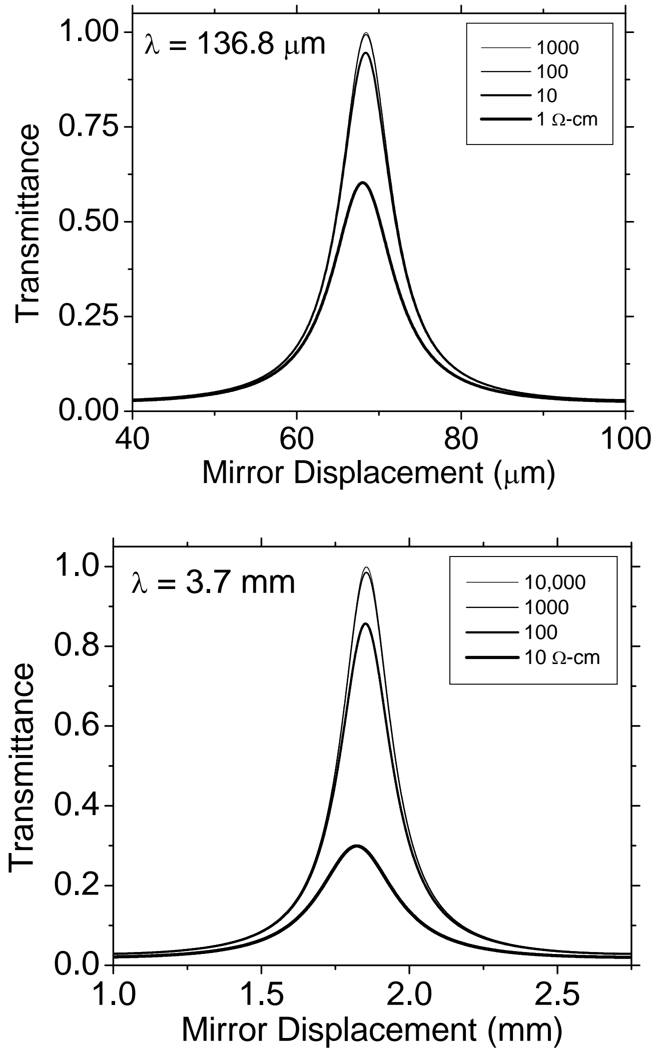

Figure 8: Resistivity dependence of Fabry-Perot resonance.

(Top) Calculated first order resonance for a Fabry Perot cavity designed for 136.8 μm wavelength and composed of a pair of 10 μm thick silicon flats having different resistivities. The curves for the highest two resistivity values are indistinguishable. (Bottom) Same, except the design wavelength is 3.7 mm and the silicon thicknesses are 270 μm.

The resonance full-width half-maximum increases (and finesse degrades) with η'' as shown in figure 9. When full-width half-maximum is plotted in terms of silicon resistivity, one

finds that at sub-mm wavelengths the free-carrier absorption significantly degrades system finesse below about 100 Ω-cm. Fortunately, float-zone silicon with resistivity as high as 10,000 Ω-cm is an item of commerce.

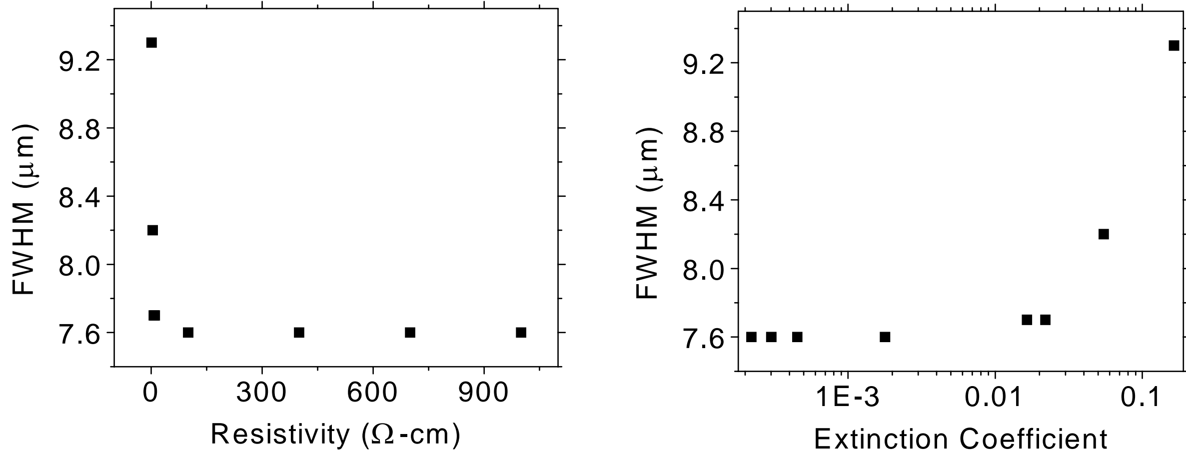

Figure 9: Full-width half-maximum as a function of the extinction coefficient and resisitivity.

Calculations of a resonance peak from a scanning Fabry-Perot are designed for 136.8 μm wavelength and composed of a pair of 10 μm silicon wafers.

(Left) Full-width half-maximum versus resistivity. (Right) Full-width half-maximum versus extinction coefficient.

Finesse Degradation

The experimental finesse F (equation 14) is reduced from the value of F_R (equation 12) (which already includes fundamental absorption losses) by various technological factors, according to[17]

$$\frac{1}{F^2} = \frac{1}{{F_R}^2} + \frac{1}{{F_D}^2} + \frac{1}{{F_B}^2} + \frac{1}{{F_p}^2} + \frac{1}{{F_\vartheta}^2}, \tag{28}$$

where F_D is due to mirror surface roughness, F_B is due to bowing of the mirrors, F_P is due to misalignment non-parallelism, and F_θ is due to optical ray deviation from normal incidence. The latter factor is related to the external optical system and not specifically to technological issues regarding the manufacture of the mirrors, so that it will be neglected here. Derivations of formulas relating F_D, F_B, and F_P were presented by Chabbal[27] with nearly all subsequently published discussions ultimately traceable to this paper. An alternate determination of the influence of non-uniform mirror spacing was presented by Ulrich, Renk, and Genzel.[18] Their studies on unevenness however will not apply in our case due to limitations on finesse and the angle of inclination between the mirrors. The angle of inclination of one of the mirrors is required to be on the order of 0.1° for finesse of about 10. For a finesse of 100, the angle is then required to be less than 0.001°, which is not likely in our experiment. Due to the requirement of low finesse values for a reasonable angle between mirrors in Ulrich's formulation,[18] the formulation of Chabbal is followed in this work.

The factor F_B due to spherical bowing is determined according to

$$F_B = \frac{\lambda}{2b}, \tag{29}$$

where b is the magnitude of the bowing at the center of the mirror relative to its edges. Such bowing can occur by improper polishing (as done purposely in amateur lens making), or through thermal expansion if the edges of the mirror are clamped in a holder with different expansion coefficient. The factor F_P due to finite accuracy in adjusting the parallelism of the mirrors is given by

$$F_P = \frac{\lambda}{\sqrt{3}p}, \tag{30}$$

where p is the maximum variation in distance between the two mirrors due to the tilt. The factor F_D due to surface defects is

$$F_D = \frac{\lambda}{x\sqrt{32\ln 2}}, \tag{31}$$

where x is the mean deviation of mirror planarity due to a gaussian distribution of defects. The scattering loss caused by such defects is ignored.

CHAPTER THREE: EXPERIMENTAL DETAILS

Chemical Etching

A practical Bragg-mirror Fabry-Perot requires a more robust monolithic mirror. Anisotropic etching of silicon wafers was explored as a means of making thin silicon foils surrounded by an integrated ring of silicon as a spacer. Wafers of both <111> and <100> orientation were considered. The silicon wafers were standard cleaned, and then 500 nm of oxide was grown on them in a wet oxidation furnace at 1100 °C. The oxidized wafers were then patterned with negative photo resist to form windows for oxide etching. The back side of the silicon wafer was also protected by negative photo resist. The patterned silicon wafers were etched in buffered oxide etch solution to strip the oxide and open windows for silicon etching. After stripping the oxide within the patterned windows, the remaining photo resist was removed with acetone. Then the silicon within the windows was thinned by etching in trimethylammonium hydroxide $(CH_3)_4NOH$ (TMAH). Isopropyl alcohol was added to the TMAH solution to obtain smoother surfaces. Roughness and depth of the etched surfaces was characterized using an optical profilometer.

To investigate the photoresist process, patterned 26 μm spacers of SU8 photoresist (epoxy based) polymer were fabricated on top a silicon substrate. The spacer was characterized by optical profilometry.

Fabry-Perot Setup

Bragg stacks were built out of silicon wafers to use as Fabry-Perot mirrors. Wafers of a particular thickness and resistivity were separated by air gaps formed by spacers of mylar for sub-mm wavelengths or machined brass for millimeter wavelengths. In situations where available wafer or spacer optical thickness did not match a quarter of the wavelength for the sources available to us, thicknesses are matched as close as possible to a multiple of a quarter of those wavelengths. The Bragg stacks were joined on the outer edge using rubber cement. Specifications for mirrors used are collected in table 1. Mirrors were aligned while observing transmittance resonances recorded in real time using a Labview program as one mirror moved continuously back and forth. The alignment of the mirrors was re-adjusted until transmittance measurements observed were the sharpest possible using adjustable optical mounts. The translation stage was either a Thorlabs VX25D/M 25mm high precision motorized translation stage with a 20 nm step size or a Thorlabs LNR50S TravelMax with normal 50 nm step size. The maximum displacement in either case was 50 nm.

Table 1: Specifications for mirror design.

All values are the actual values used and not theoretical optimum values. Specifications are using various silicon wafers in conjunction with various wavelengths.

Mirror	Test Wavelength (µm)	# of Silicon Layers per mirror	Silicon Thickness (µm)	Spacer Thickness (µm)	Silicon Resistivity (Ω-cm)
A	3703.7	3	270	925	>3000
B	134.00	1	10	50	10
C	134.00	2	10	50	10
D	109.29	1	57	200	400
E	109.29	2	57	200	400

A Siemens backwards wave oscillator tunable from 75 to 110 GHz and microwave power meter were used in the collection of data in the millimeter wavelength range. The scanning Fabry-Perot was placed between horns that coupled the waveguide beam to free space. For sub-millimeter wavelength measurements, monochromatic radiation of wavelength 134.00 µm or 109.29 µm and was provided by a coherent DEOS gas laser chopped at 20 Hz. The transmitted signal was detected with a Golay cell and synchronously amplified using a lock-in amplifier. For pictures of the equipment used in this study, see the appendix.

CHAPTER FOUR: DATA ANALYSIS

Fabry-Perot Spectra

Figure 10 presents a comparison of the 1st order resonance with the model calculation for the Fabry-Perot with *A* mirrors at a wavelength of 3.7 mm. The experimentally determined finesse is 422, while the value calculated for this structure is 960. This theoretical finesse for three periods is less than the finesse calculated for three periods shown in figure 7 because this calculation is for the actual resistivity of the wafers used (see table 1 for *A* mirrors). The resonance width is ~5 microns in mirror travel, so that there is obviously a strong sensitivity to alignment. The resonance width is already less than the nominal machining accuracy for the brass air-gap spacers.

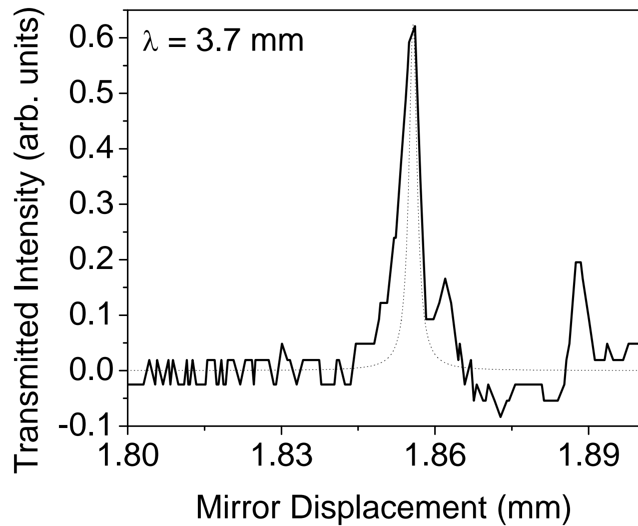

Figure 10: Experimental (solid) and theoretical (dotted) Fabry-Perot resonance. Silicon Bragg mirrors *A* are used.

Figure 11 (Top) presents experimental resonance data (solid curve) for a scanning Fabry-Perot cavity formed by a pair of *B* mirrors. The finesse of about 4.5 is seen to be about a factor of 2 worse than the theoretical prediction of 9 (dotted curve). The calculation was done for an ideal spacer thickness of 34.2 μm, which would have matched the optical thickness of the silicon used, but the actual thickness of the spacers was 50 μm. Calculation for that actual thickness improves the agreement with experiment only slightly, however.

Figure 11 (Bottom) is experimental data obtained using *C* mirrors. Although a sharpening of the resonances and increase of the finesse to a value of about 6 is observed, the difference between experiment and prediction (dotted curve) has increased by a factor of 17 to a finesse of 103. Again, calculation for the actual spacer thicknesses fails to improve the agreement significantly. The cause may be poor alignment of the individual silicon layers within

each Bragg mirror. The predicted finesse in figure 11 is significantly lower than the ideal case of figure 6 because the figure 11 calculations were performed for the actual low resistivity of the wafers used. The actual distance between mirrors is approximately 1 cm, which indicates the observed resonances are approximately of order 150. A small cavity length could not be achieved due to the experimental geometry.

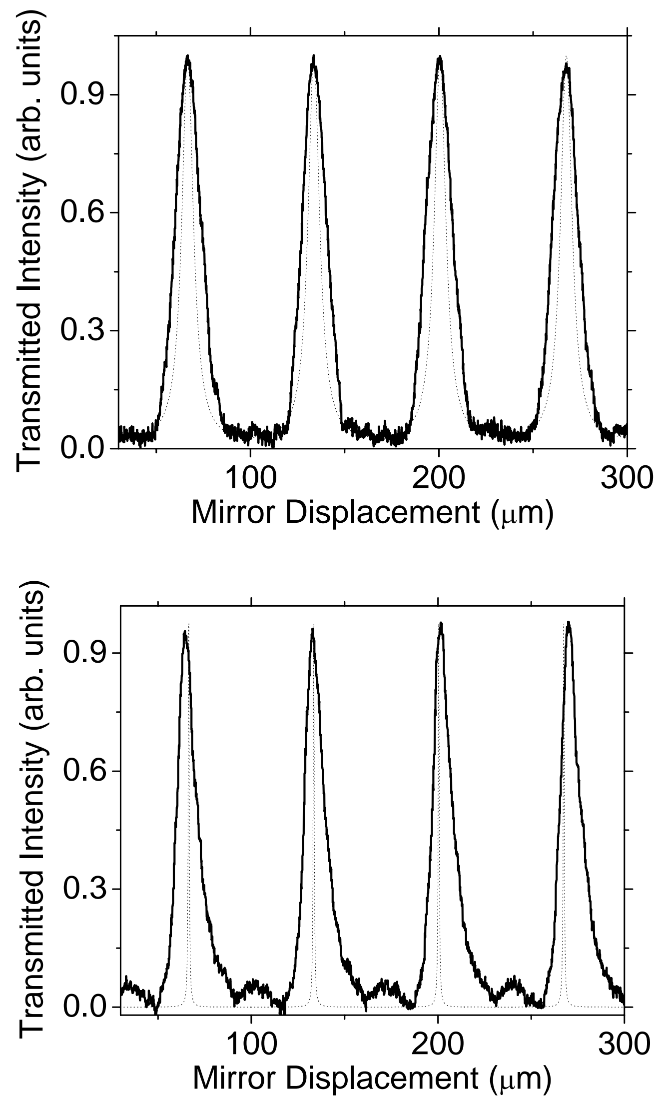

Figure 11: Experimental (solid) and theoretical (dotted) data at a wavelength of 134.00 μm. Sub-mm wave scanning Fabry-Perot using (Top) Bragg mirrors B (Bottom) Bragg mirrors C.

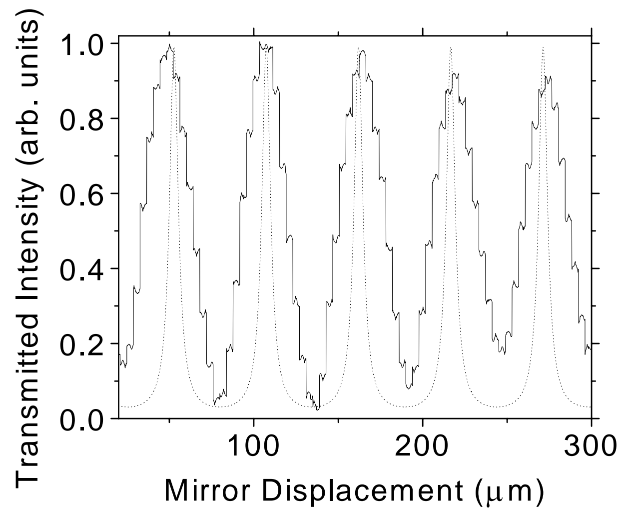

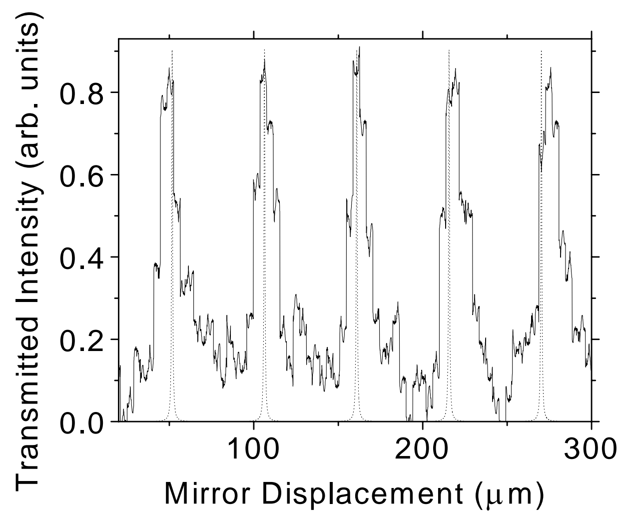

Figure 12: Experimental (solid) and theoretical (dotted) data at a wavelength of 109.29 μm. Sub-mm wave scanning Fabry-Perot using (Top) Bragg mirrors D (Bottom) Bragg mirrors E.

Figure 12 (Top) presents resonance data (solid line) for a Fabry-Perot using D mirrors. A finesse value of 1.7 is observed, which is smaller than the calculated prediction by a factor of ~5.

For a Fabry-Perot with E mirrors (figure 12, Bottom) a finesse of 5.6 is observed which is now a factor of 15 smaller than the theoretical value. Finesse has increased with the number of periods, from mirrors D to mirrors E, but not as fast as predicted. Again, inaccuracies in the construction of the multiple layers are suspected. The data in figure 12 contains steps that appear due to the Labview data acquisition program only sampling when the scanning Fabry-Perot mirror has stopped moving and not continuously. With the lack in accuracy of the data due to the large steps, further analysis of the finesse wasn't completed. The data is presented here simply for completeness.

Chemical Etchcing Results and Finesse Factors

Silicon wafers of 10 μm thickness are flexible and are subject to considerable distortion as a consequence of differential thermal expansion. Supposing such a wafer to be rigidly clamped in an aluminum ring gives a probable upper bound for the degree of bowing for a given temperature change. The linear expansion coefficient for silicon is[36] $2.6 \times 10^{-6}\ K^{-1}$. For aluminum it is $24 \times 10^{-6}\ K^{-1}$. The differential thermal expansion for a 1 cm diameter silicon wafer that undergoes a 20° C temperature change is then ~ 4 μm, which results in a bowing of the silicon b of order 100 μm. Equation 29 then predicts an F_B value of only 0.5 at 100 μm wavelength. Even at 3 mm wavelength, F_B is only 15. Thus, thermal deformation may strongly degrade the total finesse F, and the manufacturing method must carefully consider this effect. In this study none of the silicon layers were rigidly bound, the mechanically independent spacers were attached at their edges with flexible rubber cement, and both assembly and characterization

were done in a controlled laboratory environment. Thus, there is no strong reason to suspect that F_B was the limiting factor in the experimental finesse.

The surface roughness x of commercial polished wafers, such as were used in this study, is of order 2 nm, giving F_D ~ 10,000 (equation 31) at 100 μm wavelength and ~300,000 at 3 mm wavelength. Thus, F_D is unimportant in this case. The situation will be similar for the photoresist process, but the situation with etched wafers is considerably different. Figures 13 and 14 present depth profiles for our etching experiments. Besides being very slow, etching of <111> oriented wafers produced a poor surface finish with characteristic roughness x of magnitude 1 μm. On the other hand, <100> etched wafers produced a surface roughness x less than 100 nm, for which F_D is ~200 at 100 μm wavelength and ~6,000 at 3 mm. Thus surface roughness of etched wafers would reduce the total finesse by about 2 orders of magnitude at sub-millimeter wavelengths from the high values predicted on the basis of F_R alone. Still, a finesse of 200 would exceed the highest values reported for sub-mm wave Fabry-Perot spectrometers based on metal mesh.

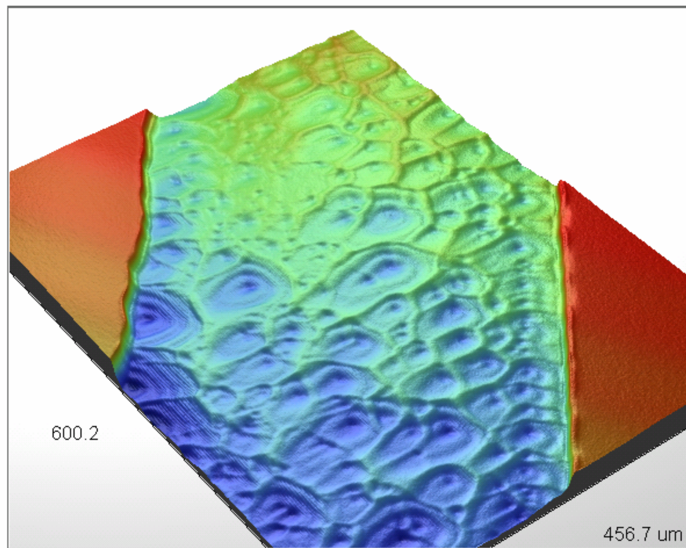

Figure 13: Depth profiling image for 60 minute patterned etch on <111> oriented silicon.

The etch depth produced is only ~1.2 μm and the resulting surface is rough.

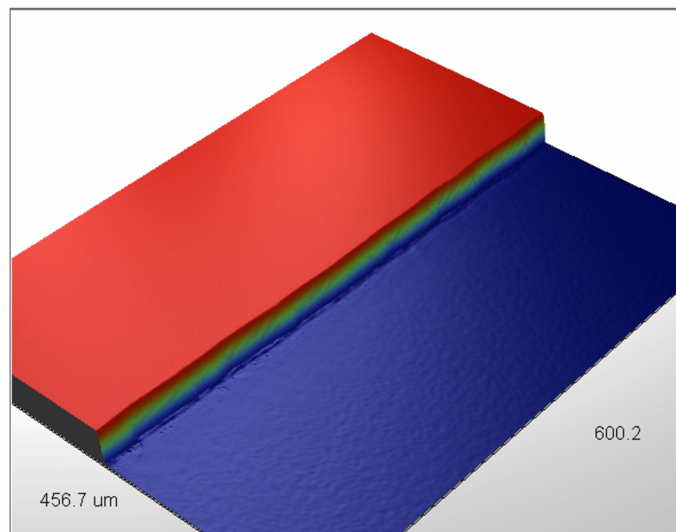

Figure 14: Image for 60 minute patterned etch on <100> oriented silicon.

Where the achieved depth is ~21 μm and the surface is comparatively smooth.

The last factor we consider is F_P. In our millimeter wavelength demonstration, standard off-the-shelf wafers were used. The parallelness of commercial double side polished wafers is rarely better than 1 μm over transverse dimensions of a few cm, and this value is a measure of the minimum p value for the complete Fabry-Perot system, giving F_P ~1,700 (equation 30) for the millimeter wavelength experiments (similar for the etching results). In order to achieve a greater order of magnitude in F_P, a smaller order of magnitude of p is required. However, the predicted F_R value for the 3000 Ω–cm wafers used was only 960, so that wafer non-parallelism was unlikely to be a limiting factor in that experiment. The ultrathin 10 μm wafers used in the experiment at 134 μm had been prepared to a higher degree of parallelism than usual double side polished wafers. Assuming parallelism to be better than 100 nm (it was not specified or measured) gives an F_P value of ~600 (again similar for the etching results), which is very much greater than the calculated F_R value of 100. We note that these F_P values are upper bounds. It is unlikely that the pair of mirrors in our sub-mm wave Fabry-Perot experiment could have been aligned to better than 1 μm, giving a more realistic F_P value of 60 for the sub-mm wave experiment. This is still much higher than the measured F value of 6. As in the millimeter wavelength range, a smaller order of magnitude of p is required in order to increase F_P by an order of magnitude. The SU8 photoresist spacers fabricated on the silicon as of yet have not shown ideal surface flatness. Spin coating photoresist on silicon can ideally achieve a small level of surface variations on the order of ~10 nm.[37] This indicates that parallelism of the Bragg mirrors created by spin coating spacers are ultimately only limited by the parallelism of the wafers used. This parallelism as stated before can ideally be ~1 μm for thick wafers to be used in

the millimeter wavelength range or ~100 nm for thin wafers to be used in the sub-mm range. These also give the same corresponding finesse limitations F_P as discussed earlier.

CHAPTER FIVE: DISCUSSION

Tables 2 and 3 summarize the results presented in the previous chapter. The factor F_B is ignored because we do not consider it to have been important in our demonstration, and because we assume that the potential bowing due to differential thermal expansion can be engineered out. Likewise, F_θ is ignored, since this relates to the entire optical system, not the manufacturing tolerances of the Fabry-Perot itself. The values given for the experiment reflect the actual mirrors built. The values for the two proposed processes are somewhat speculative given that complete Bragg mirrors have yet to be constructed by either method. The F_P factors are upper bounds, since we consider only non-parallelism due to manufacturing effects, assuming that the two mirrors in the Fabry-Perot can be otherwise perfectly aligned. F is the limiting finesse value. The limiting finesse factors for each case are colored blue in table 2 and 3.

Table 2: Estimated finesse factors for 100 μm wavelength.

	F_R	F_D	F_P	F	F_{exp}
Experiment	100, 2 periods	10,000	600	100	6
Etching process	~78,000, 6 periods	200	600	200	----
Photoresist process	~78,000, 6 periods	10,000	600	600	----

Table 3: Estimated finesse factors for 3 mm wavelength.

	F_R	F_D	F_P	F	F_{exp}
Experiment	960, 3 periods	300,000	1,700	960	422
Etching process	~16,500, 6 periods	6,000	1,700	1,700	----
Photoresist process	~16,500, 6 periods	300,000	1,700	1,700	----

From tables 2 and 3, we note that F_R value limits the total finesse in the experiments studied here. That $F_{exp} << F_R$ for the sub-mm wave experiment indicates that non-technological factors such as F_θ were likely important. This suggests that if a means can be found to securely bond commercial ultra-thin wafers into a multilayer Bragg stack, then a high finesse sub-mm wave Fabry-Perot spectrometer is possible in principle.

The etching process seems mainly limited by the resulting surface quality. Etched <100> surfaces need to be characterized by atomic force microscopy to obtain a better measure of the final surface quality. In any case, a sub-mm wave Fabry-Perot based on etched Bragg mirrors should still be competitive with the best metal mesh systems.

The photoresist process appears mainly limited by the flatness of the silicon wafers as with the etching process. Ideal surface variations of the photoresist was not achieved here but is believed to be reachable by spin coating. With ideal surface variation of the photoresist spacer, the parallelness factor F_P depends only on the silicon wafers themselves. However, additional experiments should be done to better establish the limits.

Figures 15 and 16 present a compilation of published predicted and measured finesse values for Fabry-Perots based on metal mesh. Also plotted as solid symbols are our predictions for Fabry-Perots based on *A*, *C* and *E* ideal silicon Bragg mirrors and our measured finesse values for the Fabry-Perots based on *A*, *C* and *E* for the non-ideal mirrors of table 1. Both theory and experiment show that the finesse for metal mesh-based Fabry-Perots increase faster with wavelength than for silicon Bragg mirror based Fabry-Perots. If theoretical predictions can be realized, which is largely a technological manufacturing question, a Fabry-Perot for sub-mm

wavelengths based on silicon Bragg mirrors ought to give superior finesse to one based on metal mesh. Note that the maximum number of points for Bragg mirrors at sub-mm wavelengths for our points in figures 15 and 16 is two. If the number of periods can be increased to 6, an ideal Fabry-Perot based on those mirrors would have a finesse of 78,000 in the sub-mm wavelength range, according to figure 6. This exceeds the most optimistic predictions for metal mesh Fabry-Perots by more than two orders of magnitude.

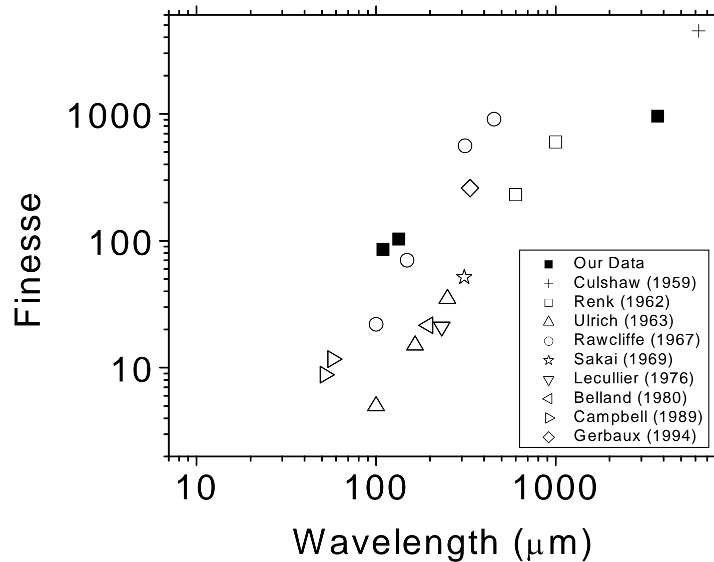

Figure 15: Theoretical finesse values vs. wavelength.

Sources are references 4,16-19, 21, 24-25, 38. Calculations for our structures *A*, *C*, and *E* assume ideal quarter wave Bragg stacks.

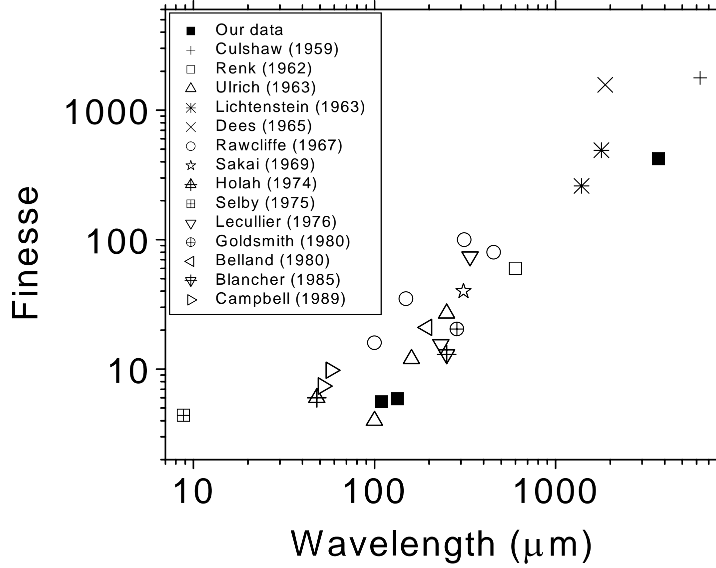

Figure 16: Empirical finesse values vs. wavelength.

Sources are references 4, 11-12, 16-19, 21-26, 39. Measured values for our structures are using *A*, *C*, and *E* mirrors.

Reflectance values calculated from the measured finesse values using equation 12 are compared to other reflectance values for silicon Bragg stacks (figure 17). The values from data presented here represent lower bounds of the achieved reflectance values due to limitations in finesse as discussed earlier.

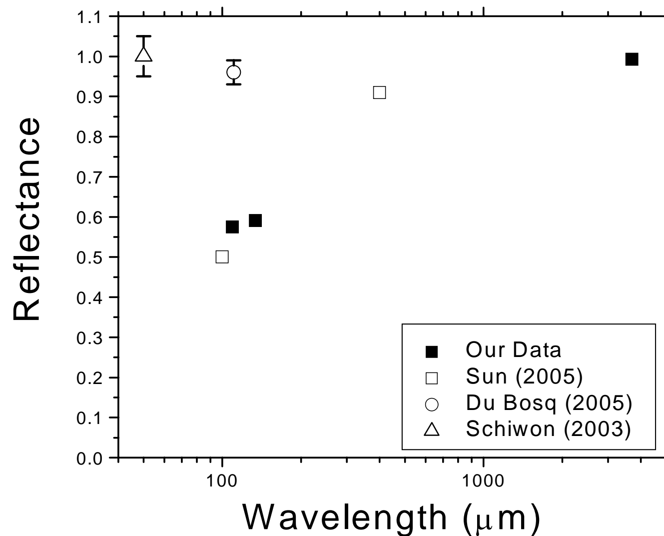

Figure 17: Measured reflectance of a silicon Bragg mirror compared to other authors.

Our sub-mm data is from 2-period Bragg stacks while the millimeter data is from 3-period Bragg stacks. Referenced data was measured using 3-periods,[8] 3-periods,[5] and 6-periods.[9]

It is shown in this work that finesse values much greater than ones measured using metal mesh can be achieved in the sub-mm and millimeter wavelength range using silicon Bragg mirrors if the technological factors such as surface roughness and unevenness of the silicon wafers can be brought done to the order of tens of nanometers. This also assumes that the Bragg mirrors in the Fabry-Perot can be made parallel such that deviation in the mirror separation is on the same order of at least tens of nanometers. The photoresist method of creating spacers is viable only if the achieved surface roughness reached the ideal level such that little tilt is caused inside the Bragg mirrors. In this scenario, the finesse will depend mainly on the parallelness of the silicon wafers as stated earlier. If these goals can be realized, using silicon Bragg mirrors in a Fabry-Perot spectrometer could still potentially give finesse values greater than 10,000. With this

Fabry-Perot system operating in low resonance order, high resolution can be achieved without the need of a complex pre-filter.

APPENDIX: EXPERIMENTAL EQUIPMENT

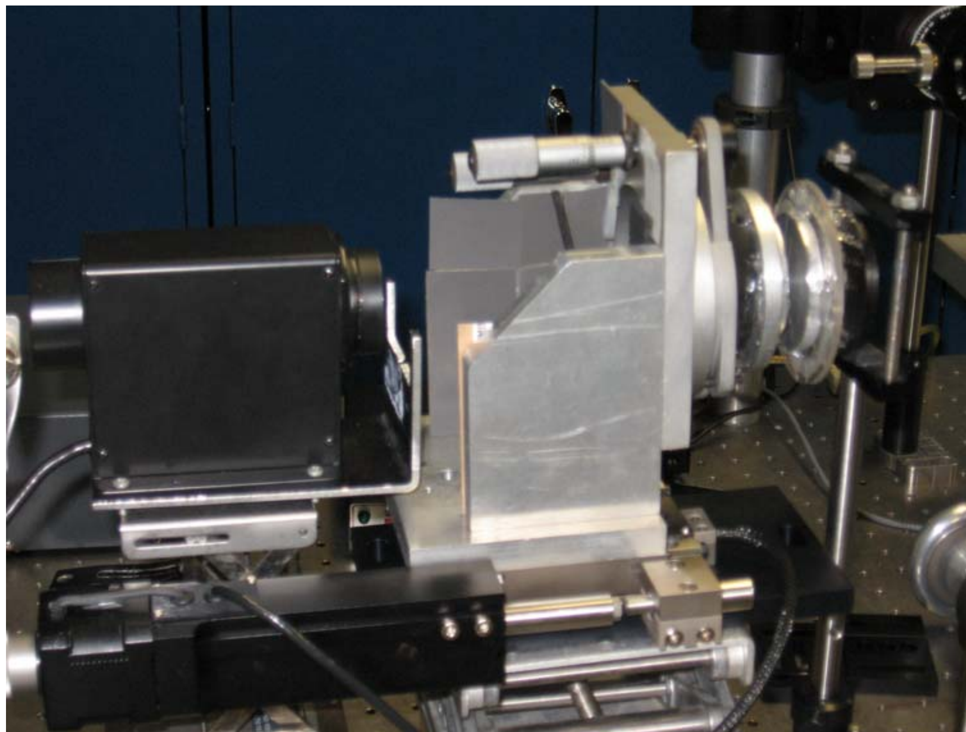

Figure 18: Fabry-Perot on Thorlabs LNR50S TravelMax with Golay cell detector.

Silicon Bragg mirrors are mounted on aluminum plates with rubber cement.

Figure 19: Far-infrared DEOS gas laser.

Figure 20: Siemens Backward Wave Oscillator (tunable millimeter wavelength source).

Figure 21: Microwave power meter and attenuator.

REFERENCES

1. R. Brodbeck, F. A. Pepe, C. Tognina, D. Bhend, E. Zimmermann, F. K. Kneubuhl, "Balloon-borne far-infrared Fabry-Perot spectrometer for astrophysical observations," Infrared Physics and Technology **39**, 393-414, 1998.

2. W. T. Reach, W. F. Wall, N. Odegard, "Infrared excess and molecular clouds: A comparison of new surveys of far-infared and H I 21 centimeter emission at high galactic latitudes," The Astrophysical Journal **507**, 507-525, 1998.

3. J. E. Harries, "Atmospheric radiometry at submillimeter wavelength," Appl. Optics **19**, 3075-3081, 1980.

4. R. D. Rawcliffe, C. M. Randall, "Metal mesh interference filters for the far infrared," Appl. Optics **6**, 1353-1358, 1967.

5. T. W. Du Bosq, A. V. Muravjov, R. E. Peale, and C. J. Fredricksen, "Multi-layer silicon cavity mirrors for the far-infrared p-Ge laser," Appl. Optics **44**, 7191-7195, 2005.

6. T. W. Du Bosq, A. V. Muravjov, and R. E. Peale, "High reflectivity intracavity Bragg mirrors for the far-infrared p-Ge laser," *Terahertz for Military and Security Applications II,* ed.by R. J. Hwu, D. L. Woolard, Proc. SPIE **5411**, 167-173, 2004.

7. T. W. Du Bosq, E. W. Nelson, A. V. Muravjov, D. A. Walters, G. Subramanian, K. B. Sundaram, R. E. Peale, N. Tache, D. B. Tanner, C. J. Fredrickson, "Etalon, lamellar, and Bragg intracavity wavelength selecting mirrors for the far-infrared p-Ge laser," OSA meeting, *Optics in the Southeast*, Orlando, 2003.

8. H. Sun, W. Shi, Z. Fu, Y. J. Ding, "Bragg reflectors and 2-D photonic crystals in the THz region," *Terahertz for Military and Security Applications III,* ed. by R. J. Hwu, D. L. Woolard, M. J. Rosker, Proc. SPIE **5790**, 104-115, 2005.

9. R. Schiwon, G. Schwaab, E. Brundermann, M. Havenith, "Far-infrared multilayer mirrors," Appl. Phys. Lett. **83**, 4119-4121, 2003.

10. L. D. Landau, E. M. Lifshitz, *Electrodynamics of Continuous Media 2nd Edition*, Ch. X, Sec. 87, Elsevier, Butterworth Heineman, Amsterdamn, 1984.

11. P. F. Goldsmith, H. Schlossberg, "A Quasi-optical Single Sideband Filter Employing A Semiconfocal Resonator," IEEE Trans. Microwave Theory and Techniques **28**, 1136-1139, 1980.

12. M. Lichtenstein, J. J. Gallagher, and R. E. Cupp, “Millimeter Spectrometer Using a Fabry-Perot Interferometer,” Rev. Sci. Instruments **34**, 843-846, 1963.

13. P. G. Wannier, J. A. Arnaud, F. A. Pelow, A. A. M. Saleh, “Quasioptical band-rejection filter at 100 GHz,” Rev. Sci. Instruments **47**, 56-58, 1976.

14. P. E. Clegg et al., “The ISO long-wavelength spectrometer,” Astronomy and Astrophysics **315**, L38-L42, 1996.

15. Poglitsch, J. W. Beeman, N. Geis, R. Genzel, M. Haggerty, E. E. Haller, J. Jackson, M. Rumitz, G. J. Stacey and C. H. Townes, “The MPE/UCB far-infrared imaging Fabry-Perot interferometer (FIFI),” Intl. J. Infrared and Millimeter Waves **12**, 859, 1991.

16. K. Sakai, T. Fukui, Y. Tsunawaki, H. Yoshinaga, “Metallic Mesh Bandpass Filters and Fabry-Perot Interferometer for the Far Infrared,” Jpn. J. Appl. Phys. **8,** 1046-1055, 1969.

17. P. Belland, J. C. Lecullier, “Scanning Fabry-Perot interferometer performance and optimum use in the far infrared range,” Appl. Optics **19** 1946-1952, 1980

18. R. Ulrich, K. F. Renk, L. Genzel, “Tunable submillimeter interferometers of the Fabry-Perot type,” IEEE Microwave Theory and Techniques **11**, 363-371, 1963.

19. K. F. Renk, L. Genzel, “Interference filters and Fabry-Perot interferometers for the far-infrared,” Appl. Optics **1**, 643-648, 1962.

20. E. A. M. Baker, B. Walker, “Fabry-Perot interferometers for use at submillimetre wavelengths,” J. Phys. E: Sci. Instrum. **15**, 25-32, 1982.

21. J. C. Lecullier, G. Chanin, “A scanning Fabry-Perot interferometer for the 50-1000μm range,” Infrared Physics **16**, 273-278, 1976.

22. H. Blancher, G. Bachet, R. Coulon, D. Aubert, “A far infrared scanning plane Fabry-Perot spectro interferometer,” Infrared and Millimeter Waves **6**, 53-62, 1985.

23. G. D. Holah, J. P. Auton, “Interference filters for the far infrared,” Infrared Physics **14**, 217-229, 1974.

24. M. F. Campbell, L. Haser, S. Drapatz, “Fabry-Perot etalons as prefilters for astronomical far-infrared fourier transform spectroscopy,” Infrared Physics **29**, 947-959, 1989.

25. W. Culshaw, “High resolution millimeter wave Fabry-Perot interferometer,” IRE Trans. Microwave Theory and Techniques **8**, 182-189, 1960.

26. J. W. Dees, A. P Sheppard, “Fabry-Perot interferometers at 168 Gc/s,” IEEE Trans. Instrumentation and Measurment **IM-14**, 52-58, 1965.

27. P. R. Chabbal, “Finesse Limite D’un Fabry-Perot Forme De Lames Imparfaites,” *J. Phys. Radium* **19**, 295-300, 1958.

28. E. Hecht and A. Zajac, *Optics 4th Printing*, Ch. 9, Addison-Wesley, Reading, 1979.

29. M. Bass, *Handbook of Optics: Fundamentals, Techniques, & Design Vol I*, 42.10-42.11, McGraw-Hill, New York, 1995.

30. H. A. Macleod, *Thin-Film Optical Filters*, 19-25, American Elsevier, New York, 1969.

31. E. W. Loewenstein, D. R. Smith, and R. L. Morgan, “Optical constants of far infrared materials 2: Crystalline solids,” Appl. Optics **12**, 398, 1973.

32. Peter Bruesch, *Phonons: Theory and Experiments II,* p.57, Springer-Verlag, Berlin Heidelberg, 1987.

33. H. Kahn, “Theory of the Infrared Absorption of Carriers in Germanium and Silicon,” *Phy. Rev.* **97**, 1647-1652, 1955.

34. Frederick Seitz, *The Modern Theory of Solids*, Dover, New York, 1987.

35. S. M. Sze, *Physics of Semiconductor Devices 2nd ed.*, Ch. 1, Sec. 1.5, Appendix G, Wiley-Interscience, New York, 1981.

36. Y. Okada, Y. Tokumaru, "Precise determination of lattice parameter and thermal expansion coefficient of silicon between 300 and 1500 K," J. Appl. Phys. **56**, 314-320, 1984.

37. S. Wolf and R. N. Tauber, *Silicon Processing for the VLSI Era: Volume 1.*, Chapter 12, p. 430-432, Lattice Press, California, 1986.

38. X. Gerbaux, A. Hadni, M. Josse, “The possibility of new high-transmission, high-finesse, Perot-Fabry interferometers for far IR spectroscopy,” Infrared and Millimeter Waves **15**, 775-783, 1994.

39. M. J. Selby, P. R. Jorden, A. D. MacGregor, “A helium cooled Fabry-Perot interferometer for infrared and astronomical spectroscopy,” Infrared Physics **16**, 317-323, 1976.